11-7-2021

Optically Active Selenium Vacancies in $BaGa_4Se_7$ Crystals

Brian C. Holloway
Air Force Institute of Technology

Timothy D. Gustafson
Air Force Institute of Technology

Christopher A. Lenyk
Air Force Institute of Technology

Nancy C. Giles
Air Force Institute of Technology

Kevin T. Zawilski
BAE Systems

See next page for additional authors

Recommended Citation

B. C. Holloway, T. D. Gustafson, C. A. Lenyk, N. C. Giles, K. T. Zawilski, P. G. Schunemann, K. L. Averett, L. E. Halliburton; Optically active selenium vacancies in BaGa4Se7 crystals. Journal of Applied Physics 7 November 2021; 130 (17): 173104. https://doi.org/10.1063/5.0067667

Journal of Applied Physics

RESEARCH ARTICLE | NOVEMBER 02 2021

Optically active selenium vacancies in $BaGa_4Se_7$ crystals

B. C. Holloway; T. D. Gustafson ; C. A. Lenyk ; N. C. Giles ; K. T. Zawilski ; P. G. Schunemann ; K. L. Averett ; L. E. Halliburton

Journal of Applied Physics 130, 173104 (2021)
https://doi.org/10.1063/5.0067667

Journal of Applied Physics ARTICLE scitation.org/journal/jap

Optically active selenium vacancies in $BaGa_4Se_7$ crystals

Cite as: J. Appl. Phys. **130**, 173104 (2021); doi: 10.1063/5.0067667
Submitted: 18 August 2021 · Accepted: 2 October 2021 ·
Published Online: 2 November 2021

B. C. Holloway,[1] T. D. Gustafson,[1,a)] C. A. Lenyk,[1] N. C. Giles,[1] K. T. Zawilski,[2] P. G. Schunemann,[2] K. L. Averett,[3] and L. E. Halliburton[4,a)]

AFFILIATIONS

[1]Department of Engineering Physics, Air Force Institute of Technology, Wright-Patterson Air Force Base, Ohio 45433, USA
[2]BAE Systems, Nashua, New Hampshire 03061, USA
[3]Air Force Research Laboratory, Materials and Manufacturing Directorate, Wright-Patterson Air Force Base, Ohio 45433, USA
[4]Department of Physics and Astronomy, West Virginia University, Morgantown, West Virginia 26506, USA

[a)]**Authors to whom correspondence should be addressed:** Timothy.Gustafson@protonmail.com and Larry.Halliburton@mail.wvu.edu

ABSTRACT

Barium gallium selenide ($BaGa_4Se_7$) is a recently developed nonlinear optical material with a transmission window extending from 470 nm to 17 μm. A primary application of these crystals is the production of tunable mid-infrared laser beams via optical parametric oscillation. Unintentional point defects, such as selenium vacancies, cation vacancies (barium and/or gallium), and trace amounts of transition-metal ions, are present in $BaGa_4Se_7$ crystals and may adversely affect device performance. Electron paramagnetic resonance (EPR) and optical absorption are used to identify and characterize these defects. Five distinct EPR spectra, each representing an electron trapped at a selenium vacancy, are observed at low temperature (there are seven crystallographically inequivalent selenium sites in the crystal). One spectrum is stable at room temperature and is present before illumination. The other four are produced at lower temperatures with 532 nm laser light and are thermally unstable at room temperature. Each S = 1/2 singly ionized selenium vacancy has a large, nearly isotropic, hyperfine interaction with ^{69}Ga and ^{71}Ga nuclei at one neighboring Ga site. A significant portion of the unpaired spin resides in a 4s orbital on this adjacent Ga ion and gives principal values of the hyperfine matrices in the 3350–6400 MHz range. Broad photoinduced optical absorption bands in the visible and near-infrared are assigned to the selenium vacancies.

I. INTRODUCTION

Growth of new, and often more complex, nonlinear optical (NLO) crystals is a key enabling technology that allows increasingly versatile laser-based devices to be developed for use from the ultraviolet to the mid-infrared and beyond.[1–4] Present NLO applications include second harmonic generation, tunable optical parametric oscillation, and terahertz generation. NLO crystals are also expected to play important roles in the emerging fields of quantum information processing.[5,6] A recent success has been the "discovery" of $BaGa_4Se_7$ crystals, with a room temperature transmission window from 470 nm to 17 μm. Yao *et al.*[7] and Badikov *et al.*[8] reported the growth of these crystals in 2010. Since then, the use of this material as an optical parametric oscillator (OPO) has been widely explored.[9–18] Its potential for use in terahertz generation has also received attention.[19–22] Biaxial $BaGa_4Se_7$ crystals have large nonlinear optical coefficients, suitable birefringence, and a high threshold for laser damage.[23–26] In an early demonstration of the material's capabilities, Kostyukova *et al.*[11] pumped a $BaGa_4Se_7$ OPO at 1.064 μm and produced output over a broad range (2.7–17 μm). Because of the wide bandgap of these crystals, intrinsic two-photon absorption loss is small when the pump wavelength is 1.064 μm.

Unwanted optical absorption from point defects can be a significant problem for many nonlinear optical materials, including $BaGa_4Se_7$. For example, to realize maximum output power from an OPO, absorption bands located near the pump wavelength must be minimized. The defects do not need to be thermally stable at room temperature since the photoinduced production of short-lived

charge states may introduce transient absorption features that affect device performance in steady-state applications or applications with high repetition rates. If a NLO crystal is to perform optimally in devices, the identities and properties of the more common defects in the material must be established and the processes by which the defects are created and eliminated must be determined. The defect-identification goal is best achieved by using electron paramagnetic resonance (EPR),[27–29] an experimental technique that has both the sensitivity and resolution needed to construct detailed atomic-scale models of defects at the wavefunction level. Typical unintentional point defects encountered in NLO crystals are anion and cation vacancies, antisites, and transition-metal impurities. Anion vacancies are especially important as they are often a dominant defect in optical materials. When present, these vacancies produce optical absorption bands with large oscillator strengths and they introduce changes in electrical and thermal conductivity.

In the present paper, we describe the production and characterization of singly ionized selenium vacancies (i.e., donors) in $BaGa_4Se_7$ crystals. Holes trapped by cation vacancies, most likely barium vacancies, are also investigated. Selenium vacancies are formed during growth, with most initially in the nonparamagnetic doubly ionized charge state (V_{Se}^{2+}). Since the crystals are electrically neutral, the selenium vacancies are compensated by acceptors such as cation vacancies and impurities on cation sites. For example, one Ba^{2+} vacancy will compensate one missing Se^{2-} ion and two Ga^{3+} vacancies will compensate three missing Se^{2-} ions. During illumination, the selenium vacancies trap electrons. Singly ionized, and thus EPR-active, selenium vacancies (V_{Se}^{+}) with one unpaired electron are produced when the $BaGa_4Se_7$ crystal is exposed to 532 nm laser light while being held at low temperature. Of the five V_{Se}^{+} spectra we observe, only one was present before exposure to laser light. The other four V_{Se}^{+} spectra are photoinduced. We provide a detailed analysis of the EPR spectra from these five V_{Se}^{+} vacancies. Each paramagnetic vacancy has a large interaction with a neighboring ^{69}Ga or ^{71}Ga nucleus. The resulting hyperfine patterns are complex because the energies of these interactions are comparable to the energy of the microwave photons used in the EPR spectrometer. This gives highly asymmetric sets of hyperfine lines around $g \approx 2.0$. We also report photoinduced optical absorption bands peaking between 430 and 750 nm at 80 K (these bands accompany the formation of the singly ionized selenium vacancy EPR spectra). A luminescence and optical absorption study by Yelisseyev *et al.*[30] is the only previously published report that investigates point defects in $BaGa_4Se_7$ crystals.

II. EXPERIMENTAL DETAILS

An undoped $BaGa_4Se_7$ crystal was grown by the horizontal gradient freeze method at BAE Systems (Nashua, NH).[31] Growth occurred in a transparent furnace using starting materials synthesized from high-purity elements by a two-temperature vapor transport process. The melting point of $BaGa_4Se_7$ is 1029 °C. After orienting with x rays, small crystals suitable for optical and EPR experiments were cut from the larger boule. Approximate dimensions of these crystals were $2.5 \times 3.2 \times 3.3\ mm^3$. The samples used in our study were not subjected to a post-growth thermal anneal in a Se-containing atmosphere.

The EPR spectra were acquired with a Bruker EMX spectrometer operating near 9.38 GHz. An Oxford Instruments ESR-900 helium-gas flow system was used to control the sample temperature and a Bruker NMR gaussmeter provided corrections for the small difference in the magnetic field at the sample and the spectrometer's Hall sensor located on a magnet pole cap. A 532 nm laser from Laserglow Technologies (Model LCS-0532-TSD) was used to convert point defects to their paramagnetic charge states. Optical absorption spectra were taken with a Cary 5000 spectrophotometer and an ultrabroadband (250 nm to 4 μm) fused-silica wire-grid polarizer from Thorlabs (Model WP25M-UB). A Cryo Industries optical cryostat with sapphire windows (Model 110-637-DND) and a Lakeshore temperature controller (Model 335) were used when taking optical absorption data below room temperature. Reflection losses were not removed from the absorption spectra.

The $BaGa_4Se_7$ crystals have a monoclinic structure (space group *Pc*) with lattice constants[7] $a = 7.6252$ Å, $b = 6.5114$ Å, $c = 14.702$ Å, and $\beta = 121.24°$ at 93 K. The *b* direction is perpendicular to the mirror plane of the crystal, β is the angle between the *a* and *c* axes, and the c^* direction is defined to be perpendicular to the *a*–*b* plane. The Ba^{2+} ions and Se^{2-} ions are much larger in size than the Ga^{3+} ions. Effective ionic radii are 1.36 Å for Ba^{2+} ions, 0.47 Å for Ga^{3+} ions, and 1.98 Å for Se^{2-} ions.[32] A portion of the $BaGa_4Se_7$ structure is shown in Fig. 1. The four Ba^{2+} ions in this figure are in the *a*–*b* plane (perpendicular to the c^* direction). They define a rectangle, indicated by the dashed lines, with sides equal to the lattice constants *a* and *b*. One Ga^{3+} ion lies above the set of four Ba^{2+} ions, and four Ga^{3+} ions lie below. In the $BaGa_4Se_7$ lattice, all the Ba sites are equivalent (each Ba^{2+} ion has 12 Se^{2-} neighbors with Ba–Se distances ranging from 3.430 to 4.199 Å). The Ga ions occupy four crystallographically inequivalent sites. As expected for a Group III ion, each Ga^{3+} forms a distorted

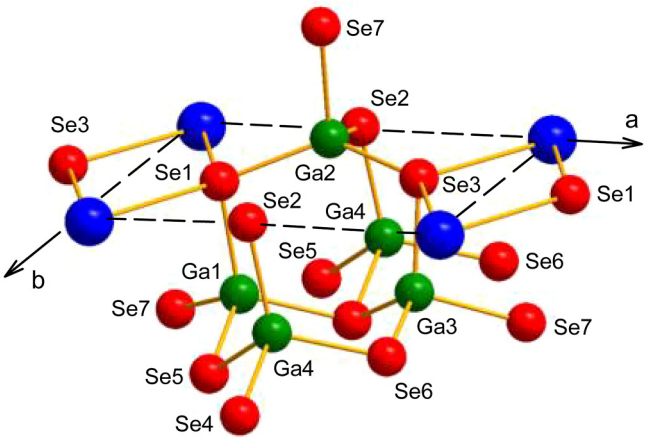

FIG. 1. A ball-and-stick representation of a portion of the monoclinic $BaGa_4Se_7$ crystal. The barium ions are blue, the gallium ions are green, and the selenium ions are red. The four Ba^{2+} ions (connected by the dashed lines) lie in the *a*–*b* plane and form a rectangle with sides equal to the lattice constants *a* and *b*.

TABLE I. The Se^{2-} ions in a $BaGa_4Se_7$ crystal have either two or three close Ga neighbors. Specific ions are identified using the labeling scheme in Ref. 7. Distances are given in Å.

Ion	Ga neighbors	Distance from Se to Ga
Se1	Ga(1), Ga(2)	2.378, 2.401
Se2	Ga(4), Ga(2)	2.368, 2.383
Se3	Ga(3), Ga(2)	2.363, 2.373
Se4	Ga(3), Ga(1), Ga(4)	2.421, 2.431, 2.488
Se5	Ga(1), Ga(4)	2.364, 2.389
Se6	Ga(3), Ga(4)	2.362, 2.387
Se7	Ga(1), Ga(3), Ga(2)	2.451, 2.451, 2.478

tetrahedron by bonding to four Se^{2-} ions. The Ga–Se distances in these tetrahedra range from 2.362 to 2.488 Å. There are seven crystallographically inequivalent Se sites in the crystal. These Se^{2-} ions have either two or three close Ga neighbors (specific neighbors and separation distances are listed in Table I).

III. EPR RESULTS

A. Electrons trapped at selenium vacancies

The EPR spectrum in Fig. 2(a) was taken from an as-grown $BaGa_4Se_7$ crystal. The same crystal was then exposed to 532 nm laser light and the EPR spectrum in Fig. 2(b) was taken. These spectra were obtained at 35 K with the magnetic field aligned along the *b* direction. The spectrum in Fig. 2(a) is complex and we wait until Sec. III B for its analysis. We first focus on the simpler photoinduced EPR spectrum that emerges when we subtract the "before light" spectrum in Fig. 2(a) from the "during light" spectrum in Fig. 2(b). This "difference" spectrum is shown in Fig. 3(a). The 532 nm light produced two types of defects (neither was present before the illumination). There is an intense single line at 329.33 mT in Fig. 3(a) due to a hole trapped on a selenium ion adjacent to a cation vacancy. This defect is described in more detail in Sec. III C. The remaining EPR lines in Fig. 3(a) are from two distinct singly ionized selenium vacancies, labeled V_{Se}^{+}(A) and V_{Se}^{+}(B). Linewidths for the two photoinduced vacancies are different: broad for V_{Se}^{+}(A) and narrow for V_{Se}^{+}(B). Since the energy of the 532 nm photons is less than the optical gap of the $BaGa_4Se_7$ crystal, we suggest that the singly ionized selenium vacancies are formed by the light when electrons are optically excited from the valence band to doubly ionized selenium vacancies (V_{Se}^{2+}). This excitation process converts nonparamagnetic V_{Se}^{2+} vacancies to paramagnetic V_{Se}^{+} vacancies. Holes left in the valence band are localized at selenium ions adjacent to cation vacancies or at impurity ions. If the crystal remains near or below 70 K, these trapped electrons and trapped holes are thermally stable after the 532 nm light is removed.

In Fig. 3(a), the concentration of defects represented by the trapped-hole spectrum is approximately $3.4 \times 10^{18}\,cm^{-3}$ and the concentrations represented by the V_{Se}^{+}(A) and V_{Se}^{+}(B) selenium

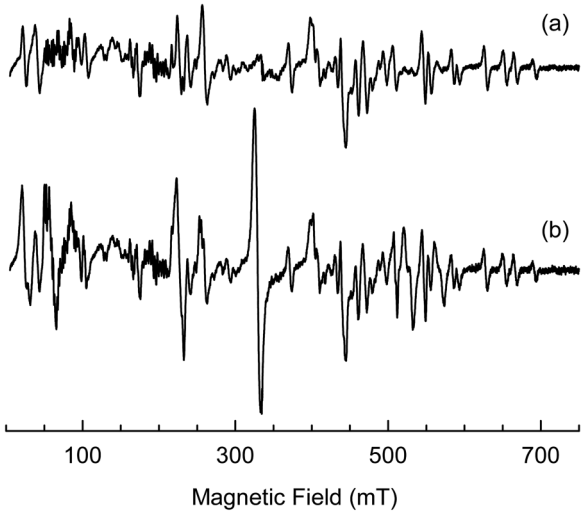

FIG. 2. EPR spectra taken from a $BaGa_4Se_7$ crystal (a) before exposure to light and (b) during exposure to 532 nm laser light. The temperature was 35 K and the magnetic field was along the *b* direction.

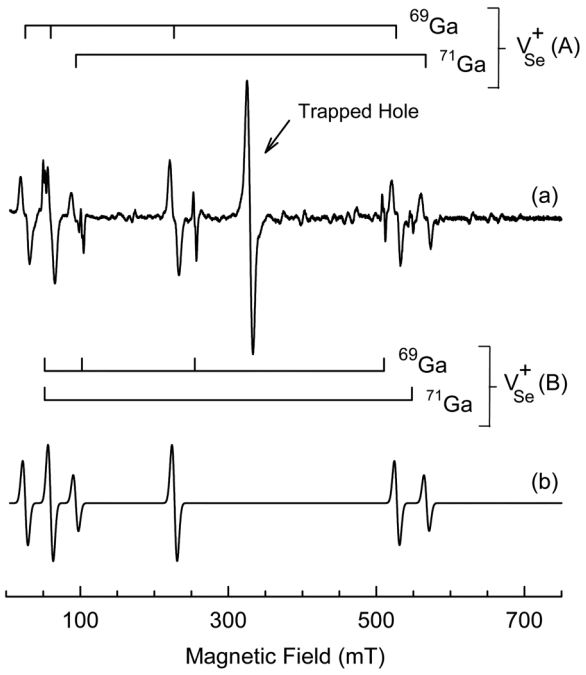

FIG. 3. (a) Photoinduced EPR spectrum from a $BaGa_4Se_7$ crystal, taken at 35 K during exposure to 532 nm laser light. The "before light" spectrum in Fig. 2(a) has been subtracted from the "during light" spectrum in Fig. 2(b). One trapped-hole center and two singly ionized selenium vacancies, V_{Se}^{+}(A) and V_{Se}^{+}(B), have been produced by the light. The magnetic field is along the *b* direction and the microwave frequency is 9.3845 GHz. (b) Simulated EPR spectrum for V_{Se}^{+}(A).

TABLE II. Magnetic field positions of lines in the EPR spectra of selenium vacancies. These data were obtained from the experimental spectra shown in Figs. 3, 6, and 7. The (F,m_F) labeling scheme is used to describe the transitions. Units are mT.

	V_{Se}^{+}(A)		V_{Se}^{+}(B)		V_{Se}^{+}(C)		V_{Se}^{+}(D)	
Transition	^{69}Ga	^{71}Ga	^{69}Ga	^{71}Ga	^{69}Ga	^{71}Ga	^{69}Ga	^{71}Ga
(2,−2) to (2,−1)	526.8	566.8	510.3	548.0	530.5	572.2	497.8	533.4
(1,−1) to (2,0)	226.6	…	255.1	…	…	…	317.8	264.8
(1,0) to (2,+1)	60.2	…	102.3	…	…	…	189.7	36.1
(1,+1) to (2,+2)	25.7	…	52.1	…	…	…	112.9	…
(1,−1) to (2,−2)	…	94.2	…	52.1	28.9	174.5	…	…

TABLE III. "Best-fit" spin-Hamiltonian parameters for singly ionized selenium vacancies in a $BaGa_4Se_7$ crystal. Line positions used in the fittings are listed in Table II (they were obtained from the EPR spectra shown in Figs. 3, 6, and 7). Units for the hyperfine values are MHz. Estimates of uncertainties are ±0.005 for the g values and ±40 MHz for the A values.

	Spin-Hamiltonian Parameters		
Defect	g value	A(^{69}Ga)	A(^{71}Ga)
V_{Se}^{+}(A)	2.000	4417	5616
V_{Se}^{+}(B)	2.024	4123	5224
V_{Se}^{+}(C)	2.061	4998	6356
V_{Se}^{+}(D)	1.951	3330	4250

vacancy spectra are approximately 11.6×10^{18} and 0.9×10^{18} cm^{-3}, respectively. These defect concentrations were obtained by comparing signal intensities to a Bruker weak-pitch EPR standard containing a known number of spins. Since the combined number of electrons trapped at selenium vacancies is more than three times greater than the number of holes trapped at cation vacancies, unseen defects must be present that serve as traps for holes. Among the candidates for these unseen defects are transition-metal ions with partially filled 3d shells or rare-earth ions with partially filled 4f shells. It is also possible that there are unseen impurities serving as electron traps.

The six lines assigned to V_{Se}^{+}(A) in Fig. 3(a) are caused by a large hyperfine interaction with ^{69}Ga and ^{71}Ga nuclei located at one Ga site adjacent to the selenium vacancy. Stick diagrams above the spectrum identify the four lines from the ^{69}Ga nuclei and the two lines from the ^{71}Ga nuclei. A slight splitting of these primary lines (i.e., the step at their centers) is caused by a much smaller unresolved hyperfine interaction with ^{69}Ga and ^{71}Ga nuclei at a second Ga site near the vacancy. The V_{Se}^{+}(A) EPR spectrum has very little angular dependence, with the highest-field lines shifting by less than 5 mT when the magnetic field direction is rotated from *b* to *a*. This establishes that a significant portion of the electron trapped by the selenium vacancy occupies a 4s orbital on the adjacent Ga ion. V_{Se}^{+}(A) can be viewed, to a first approximation, as a Ga^{2+} ($3d^{10}4s^{1}$) ion next to a selenium vacancy. The ^{69}Ga isotope has a natural abundance of 60.1% and the ^{71}Ga isotope has a natural abundance of 39.9%. They both have I = 3/2 nuclear spins

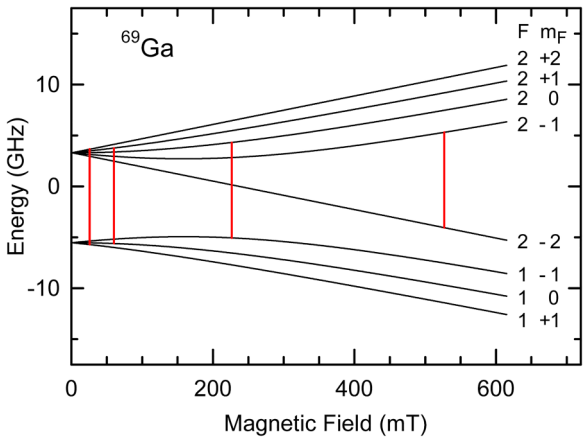

FIG. 4. Energy levels as a function of magnetic field for ^{69}Ga nuclei in the singly ionized V_{Se}^{+}(A) vacancy. The (F,m_F) labeling scheme is used for the spin states and the hyperfine parameter A is assumed to be positive. The red vertical lines represent the four ^{69}Ga transitions observed in the EPR spectrum in Fig. 3(a).

and their magnetic moments are $^{69}\mu = +2.0166\beta_n$ and $^{71}\mu = +2.5623\beta_n$ (where β_n is the nuclear Bohr magneton).[33]

A g value and the hyperfine values for the participating ^{69}Ga and ^{71}Ga nuclei are extracted from the V_{Se}^{+}(A) spectrum in Fig. 3(a). The two isotopes are treated separately by using the following spin-Hamiltonian with an S = 1/2 electron Zeeman interaction, a large isotropic I = 3/2 hyperfine interaction, and a nuclear Zeeman interaction:

$$H = g\beta \mathbf{S}\bullet\mathbf{B} + A\mathbf{I}\bullet\mathbf{S} - g_n\beta_n\mathbf{I}\bullet\mathbf{B}. \quad (1)$$

For the V_{Se}^{+}(A) spectrum, the magnitudes of gβB and 2A are similar. Introducing the raising and lowering operators allows the spin-Hamiltonian in Eq. (1) to be rewritten as

$$H = g\beta BS_z + AI_zS_z + \frac{1}{2}A(I_+S_- + I_-S_+) - g_n\beta_nBI_z. \quad (2)$$

The basis states $|M_S,m_I\rangle$, where $M_S = +1/2$ or $-1/2$ and $m_I = +3/2$, $+1/2$, $-1/2$, or $-3/2$ for each M_S value, are then used to express the spin-Hamiltonian as an 8×8 matrix. Diagonalization of this matrix gives the energies of the spin states (i.e., the eigenvalues). The four lines in Fig. 3(a) from the ^{69}Ga nuclei (at 25.7, 60.2, 226.6, and 526.8 mT) and the microwave frequency of 9.3845 GHz are input data for a least squares fitting program. Positions of these V_{Se}^{+}(A) lines are listed in Table II, along with the experimental positions of lines from the other selenium vacancies. In the fitting routine, the g and A parameters are systematically varied until the predicted line positions match the measured line positions. Table III contains the resulting "best-fit" values of these ^{69}Ga parameters. For the ^{71}Ga portion of the V_{Se}^{+}(A) spectrum, the two lines in Fig. 3(a) at 94.2 and 566.8 mT and the 9.3845 GHz microwave frequency are similarly used as input data for the fitting routine, and the results are

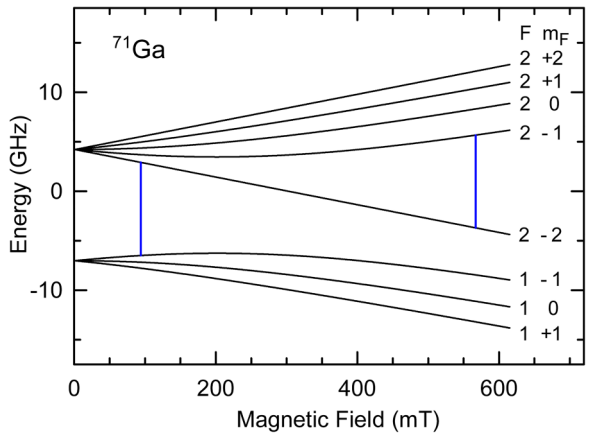

FIG. 5. Energy levels as a function of magnetic field for ^{71}Ga nuclei in the singly ionized V_{Se}^{+}(A) vacancy. The (F,m$_F$) labeling scheme for the spin states is used and the hyperfine parameter A is assumed to be positive. The blue vertical lines represent the two ^{71}Ga transitions observed in the EPR spectrum in Fig. 3(a).

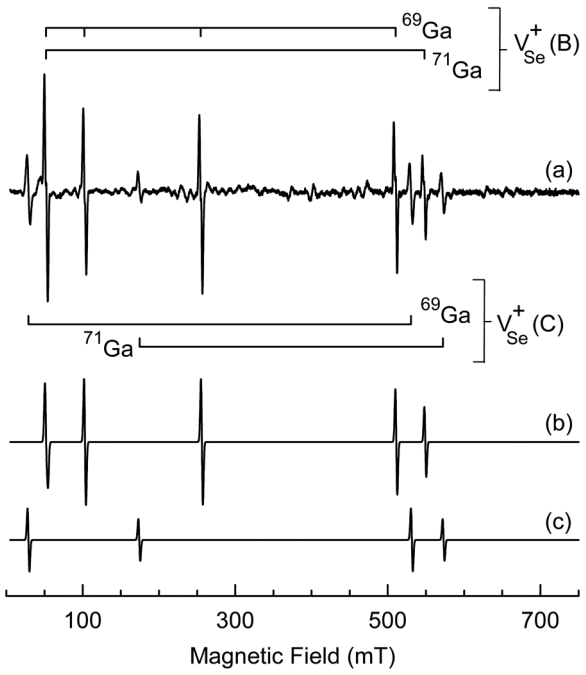

FIG. 6. (a) Photoinduced EPR spectrum taken at 35 K from a $BaGa_4Se_7$ crystal. The crystal was initially exposed at 35 K to 532 nm laser light. After removing the light, the crystal was warmed to 90 K for 1 min and then returned to 35 K for measurement. The "before light" spectrum in Fig. 2(a) has been subtracted. Two singly ionized selenium vacancies, V_{Se}^{+}(B) and V_{Se}^{+}(C), are present. The magnetic field is along the *b* direction and the microwave frequency is 9.3845 GHz. (b) Simulated EPR spectrum for V_{Se}^{+}(B). (c) Simulated EPR spectrum for V_{Se}^{+}(C).

included in Table III. The same g value is obtained from this second fitting, but the hyperfine value is larger because of the increased nuclear magnetic moment of the ^{71}Ga isotope. In Table III, the ^{71}Ga/^{69}Ga ratio of the hyperfine values for V_{Se}^{+}(A) is 1.2715. This is very close to the known value of 1.2706 for the $^{71}\mu/^{69}\mu$ ratio of the magnetic moments of the two Ga isotopes.[33] To further demonstrate that the correct spin-Hamiltonian parameters were determined, the simulated spectrum shown in Fig. 3(b) was generated with EasySpin[34,35] using the V_{Se}^{+}(A) parameters in Table III.

The large hyperfine values needed to explain the nearly isotropic V_{Se}^{+}(A) spectrum in Fig. 3(a) cause a significant mixing of the $|M_S,m_I\rangle$ states at lower magnetic fields. A more appropriate set of quantum numbers are F and m_F and the well-known Breit–Rabi analysis[36–40] of spin states is applicable. Nistor *et al.*[41] have provided a useful description of this approach in their comprehensive review of defects with very large isotropic hyperfine interactions. For I = 3/2 nuclei such as ^{69}Ga and ^{71}Ga, F has values of 1 or 2 (F = I ± 1/2) and m_F has values of F, F − 1, …, −F for each value of F. Figure 4 shows the eight energy levels (in units of GHz) as a function of magnetic field for the ^{69}Ga portion of V_{Se}^{+}(A). These curves were generated using the parameters in Table III. The (F,m$_F$) labeling scheme for the spin states is used and the four transitions observed in the EPR spectrum are shown as vertical lines (the lengths of these lines correspond to the microwave frequency). For each transition, the selection rule is $\Delta m_F = \pm 1$. Figure 5 shows the eight energy levels as a function of magnetic field for the ^{71}Ga nuclei (generated using parameters from Table III). The two vertical lines in this latter figure illustrate the transitions observed for the ^{71}Ga isotope. Again, the selection rule is $\Delta m_F = \pm 1$. Note that the zero-field splittings in Figs. 4 and 5, while different, are both equal to 2A (i.e., two times the hyperfine parameter for the respective isotope).

Although the ^{69}Ga and ^{71}Ga nuclei have similar properties (both are I = 3/2 nuclei and their nuclear magnetic moments are similar), the contributions of the two isotopes to the V_{Se}^{+}(A) spectrum in Fig. 3(a) are quite different. There are four lines from the ^{69}Ga nuclei and only two lines from the ^{71}Ga nuclei. The reason for this difference becomes obvious when the microwave frequency (9.3845 GHz) is compared to the 2A hyperfine values for ^{69}Ga and ^{71}Ga in Table III (8.834 and 11.232 GHz, respectively). The microwave frequency is greater than 2A for the ^{69}Ga nuclei and less than 2A for the ^{71}Ga nuclei. Using the (F,m$_F$) labels and referring to Figs. 4 and 5, the (1,−1) to (2,−2) transition is only seen when the microwave frequency is less than the zero-field splitting value of 2A. In contrast, the (1,+1) to (2,+2), the (1,0) to (2,+1), and the (1,−1) to (2,0) transitions are only seen when the microwave frequency is greater than the zero-field splitting value of 2A. The (2,−2) to (2,−1) transition is seen under all conditions.

After the EPR data in Fig. 3(a) were taken, the 532 nm laser light was removed, and the crystal was briefly warmed to 90 K (for 1 min) while remaining in the microwave cavity with the magnetic field along the *b* direction. The temperature was quickly returned to 35 K and the EPR data shown in Fig. 6(a) were obtained with no further exposure to laser light. Figure 6(a) is the "difference" spectrum obtained by subtracting the "before light" spectrum in

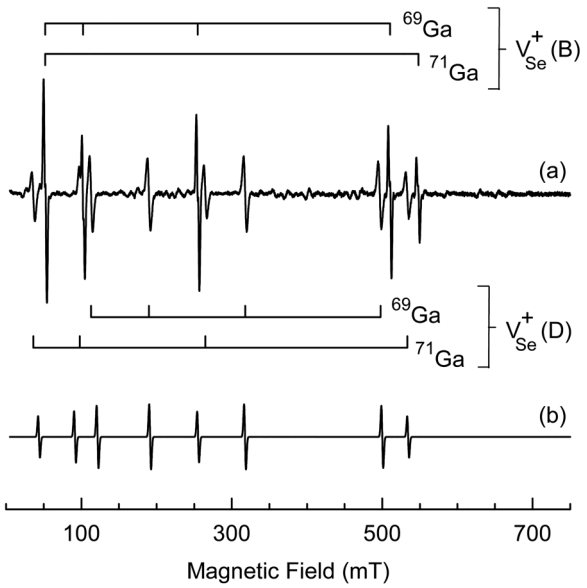

FIG. 7. (a) Photoinduced EPR spectrum taken at 35 K from a $BaGa_4Se_7$ crystal. The crystal was initially exposed at 35 K to 532 nm laser light. After taking the spectrum in Fig. 6(a), the crystal was warmed to 120 K for 1 min and then returned to 35 K for measurement. The "before light" spectrum in Fig. 2(a) has been subtracted. Two singly ionized selenium vacancies, V_{Se}^{+}(B) and V_{Se}^{+}(D), are present. The magnetic field is along the *b* direction and the microwave frequency is 9.3845 GHz. (b) Simulated EPR spectrum for V_{Se}^{+}(D).

Fig. 2(a) from the spectrum taken after heating to 90 K. Comparing the spectra in Figs. 3(a) and 6(a) shows that the heating to 90 K caused significant changes in the selenium vacancies. The trapped hole and V_{Se}^{+}(A) spectra are no longer present, the concentration of V_{Se}^{+}(B) increased by a factor of two (to 1.9×10^{18} cm^{-3}), and a new selenium vacancy, labeled V_{Se}^{+}(C), appeared with a concentration of 0.8×10^{18} cm^{-3}. Magnetic field positions for the V_{Se}^{+}(B) and V_{Se}^{+}(C) EPR lines in Fig. 6(a) are included in Table II. Using these magnetic field values and the 9.3845 GHz microwave frequency, the g and hyperfine parameters for V_{Se}^{+}(B) and V_{Se}^{+}(C) were determined by the same fitting procedure used for V_{Se}^{+}(A). The results are presented in Table III. The simulated spectra for V_{Se}^{+}(B) and V_{Se}^{+}(C) shown in Figs. 6(b) and 6(c), respectively, were generated with EasySpin[34,35] using the parameters in Table III.

Next, the $BaGa_4Se_7$ crystal was warmed to 120 K without illumination, held at this temperature for 1 min, and then returned to 35 K for measurement. Figure 7(a) shows EPR data taken with the magnetic field along the *b* direction. The "difference" spectrum in Fig. 7(a) was obtained by subtracting the initial "before light" spectrum in Fig. 2(a) from the spectrum taken after heating to 120 K. This second heating step introduced further changes in the selenium vacancies. The V_{Se}^{+}(C) spectrum disappeared and the concentration of V_{Se}^{+}(B) increased to 2.3×10^{18} cm^{-3}. A fourth selenium vacancy, labeled V_{Se}^{+}(D), appeared with a concentration of 1.4×10^{18} cm^{-3}. The combined increase in the number of V_{Se}^{+}(B) and V_{Se}^{+}(D) vacancies at 120 K is more than the decrease in the number of V_{Se}^{+}(C) vacancies. This suggests that unseen defects release electrons at this temperature, which then become trapped at selenium vacancies. Table II contains the magnetic field positions for the V_{Se}^{+}(D) EPR lines in Fig. 7(a). Using these field values and a microwave frequency of 9.3845 GHz, the g and hyperfine parameters for V_{Se}^{+}(D) were determined in the same manner as for the other three selenium vacancies, and the results are included in Table III. The simulated spectrum for V_{Se}^{+}(D), shown in Fig. 7(b), was generated with EasySpin[34,35] using the parameters in Table III.

Information about the thermal stability of the observed singly ionized selenium vacancies is provided by the data in Figs. 3, 6, and 7. The dominant selenium vacancy, V_{Se}^{+}(A), thermally decays below 90 K, V_{Se}^{+}(C) thermally decays between 90 and 120 K, and V_{Se}^{+}(B) and V_{Se}^{+}(D) are stable above 120 K, but not at room temperature. As the V_{Se}^{+}(A) vacancies thermally decay during the warming step to 90 K, the V_{Se}^{+}(B) and V_{Se}^{+}(C) vacancies grow, thus indicating that a portion of the electrons released from the less stable V_{Se}^{+}(A) vacancies move within the crystal and form the more stable singly ionized vacancies. In separate experiments, we found that the V_{Se}^{+}(A) vacancies produced at 35 K by the 532 nm laser light can be destroyed at this temperature with 633 nm laser light. The other three photoinduced selenium vacancies observed at low temperature can also be destroyed with the 633 nm light. In contrast, 1064 nm laser light has little effect on the singly ionized selenium vacancies. After the photoinduced singly ionized charge states are eliminated either by warming or optical bleaching, the selenium vacancies remain in the crystal but are no longer seen with EPR (i.e., they have reverted to a nonparamagnetic charge state).

Additional support for selenium vacancies being a primary defect in $BaGa_4Se_7$ crystals is found in the literature. Our results are consistent with several reports that suggest post-growth annealing in a Se-containing atmosphere improves crystal quality and reduces point defects. Guo *et al.*[24] significantly improved the transmittance of crystals at longer wavelengths by thermal annealing under an atmosphere of $BaGa_4Se_7$ powder vapor. Yelisseyev *et al.*[30] showed that annealing $BaGa_4Se_7$ crystals in a BaSe atmosphere greatly reduced the dominant photoluminescence (PL) band at 694 nm (1.785 eV). This latter result, when combined with our present EPR results, leads us to suggest that the 694 nm PL band, observed at 80 K, may be associated with singly ionized selenium vacancies. Yelisseyev *et al.*[30] had tentatively attributed this PL band to a barium vacancy (V_{Ba}) or a gallium-on-barium antisite (Ga_{Ba}) defect.

B. EPR spectra present in as-grown $BaGa_4Se_7$ crystals

The EPR spectrum obtained from the $BaGa_4Se_7$ crystal prior to exposure to laser light is shown in Fig. 8(a) (this is the "before light" spectrum shown earlier in Fig. 2). This spectrum was recorded at 35 K, with the magnetic field aligned along the *b* direction and a microwave frequency of 9.3845 GHz. Two sets of closely spaced lines near 75 and 200 mT are present in Fig. 8(a) and are tentatively assigned to Mn^{3+} ($3d^4$) ions.[42–44] The set of lines near 75 mT shows an approximate 7 mT hyperfine splitting from the ^{55}Mn nucleus (I = 5/2, 100% abundant) and an additional smaller 2 mT superhyperfine splitting due to ^{69,71}Ga nuclei located at one adjacent Ga site. Although not shown, an additional set of lines

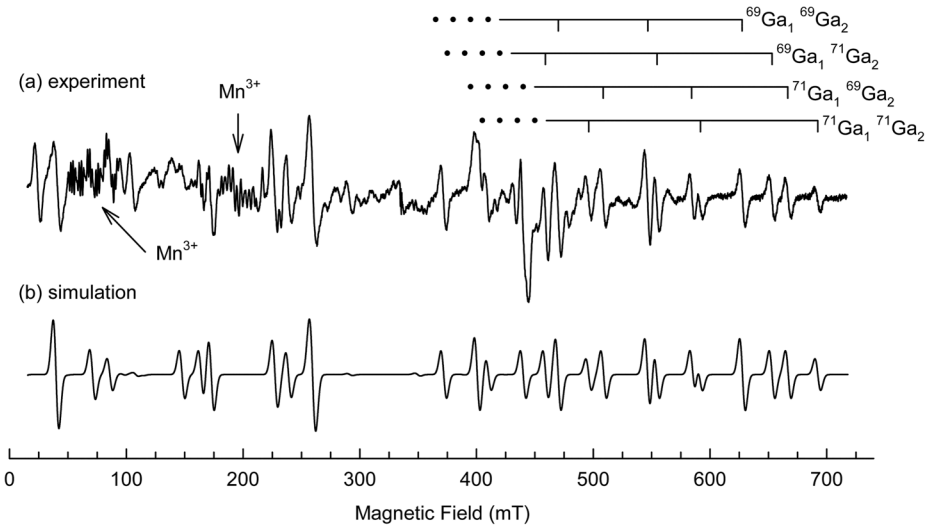

FIG. 8. EPR spectrum taken at 35 K before exposing the $BaGa_4Se_7$ crystal to laser light. The magnetic field is along the *b* direction. (a) Experimental spectrum. (b) Simulated spectrum generated using EasySpin. Stick diagrams above the experimental spectrum identify hyperfine lines associated with the different combinations of ^{69}Ga and ^{71}Ga nuclei.

from the Mn^{3+} ions is present at high field, near 890 mT, when the magnetic field is along the *b* direction. The Mn^{3+} ions in $BaGa_4Se_7$ occupy a Ga^{3+} site and are not affected by the 532 nm laser light.

Nearly all the EPR lines in Fig. 8(a), except those due to Mn^{3+}, are associated with one intrinsic defect. These lines, extending from 20 to 700 mT, are caused by large and unequal, nearly isotropic, hyperfine interactions of an unpaired electron with ^{69}Ga and ^{71}Ga nuclei at two regular lattice sites. The responsible defect is a singly ionized selenium vacancy and is labeled $V_{Se}^{+}(E)$. This defect is stable at room temperature and is observed in the as-grown $BaGa_4Se_7$ crystals before exposure to 532 nm laser light. Unlike the selenium vacancies in Sec. III A that interact primarily with one Ga neighbor, $V_{Se}^{+}(E)$ shares its unpaired spin unequally with two Ga neighbors (approximately 65.6% of the spin is on one neighbor and 34.4% is on the other neighbor). This explains the larger number of lines in the spectrum. A lack of angular dependence for $V_{Se}^{+}(E)$ indicates that the unpaired spin occupies $4s^1$ orbitals on the two adjacent Ga ions. The $V_{Se}^{+}(E)$ EPR spectrum is described by the following spin-Hamiltonian with $S = 1/2$, $I_1 = 3/2$, and $I_2 = 3/2$:

$$H = g\beta \mathbf{S} \bullet \mathbf{B} + A_1 \mathbf{I}_1 \bullet \mathbf{S} + A_2 \mathbf{I}_2 \bullet \mathbf{S} - g_n \beta_n \mathbf{I}_1 \bullet \mathbf{B} - g_n \beta_n \mathbf{I}_2 \bullet \mathbf{B}. \quad (3)$$

Electron Zeeman, hyperfine, and nuclear Zeeman terms are included. Subscripts 1 and 2 refer to the neighboring Ga sites with the larger and the smaller hyperfine interactions, respectively.

The $V_{Se}^{+}(E)$ spectrum in Fig. 8(a) consists of four superimposed groups of lines, each representing a different distribution of the ^{69}Ga and ^{71}Ga nuclei among the two participating Ga sites. Relative line intensities are determined by the natural abundances of the two isotopes. For 36.1% of the $V_{Se}^{+}(E)$ vacancies, both Ga sites have a ^{69}Ga nucleus. For 24% of the vacancies, site 1 has a ^{69}Ga nucleus and site 2 has a ^{71}Ga nucleus. Similarly, for another 24%, site 1 has a ^{71}Ga nucleus and site 2 has a ^{69}Ga nucleus. For the remaining 15.9%, both sites have a ^{71}Ga nucleus. Stick diagrams above the high field lines in Fig. 8(a) illustrate the contributions from the different combinations of isotopes. The numerical fitting capability in the EasySpin simulation program[34,35] was used to extract values for g, A_1, and A_2 from the nearly isotropic experimental spectrum. These results are listed in Table IV. Figure 8(b) shows the simulated spectrum generated with these parameters. There is good agreement between the experimental and the simulated spectra.

C. Holes trapped by cation vacancies

As shown in Fig. 3(a), a broad EPR line near 329 mT is formed when the $BaGa_4Se_7$ crystal is exposed to 532 nm laser light while being held at 35 K. With the magnetic field along the *b* direction, the width of the line is approximately 7.0 mT and its g value is 2.037. The g value of this $S = 1/2$ defect varies from 2.030 to 2.065 for other directions of the magnetic field. These small positive g shifts suggest that the responsible defect is a cation vacancy with an unpaired spin localized on one of the adjacent selenium ions. A Se^{2-} ion loses an electron and becomes a Se^{-} ion with a $4p^5$ valence shell. The effective negative charge of the cation vacancy stabilizes the hole (i.e., the missing electron) on the selenium ion, thus forming a stable defect at a sufficiently low temperature. Similar defects, referred to as acceptor-bound small polarons, have been widely studied in oxide crystals.[45–49] Trapped-hole centers of this type usually have broad optical

TABLE IV. Spin-Hamiltonian parameters for $V_{Se}^{+}(E)$ in $BaGa_4Se_7$. Values for these parameters were obtained by using EasySpin to fit the experimental spectrum in Fig. 8(a). Estimates of uncertainties are ±0.005 for the g values and ±40 MHz for the hyperfine values.

		Hyperfine parameters (MHz)			
		A_1 (Ga site 1)		A_2 (Ga site 2)	
Selenium vacancy	g value	^{69}Ga	^{71}Ga	^{69}Ga	^{71}Ga
$V_{Se}^{+}(E)$	2.013	4326	5496	2269	2883

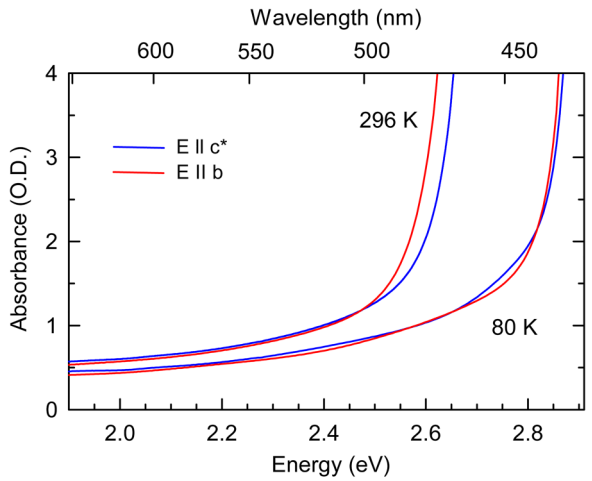

FIG. 9. Optical absorption spectra taken at 296 and 80 K from the as-grown $BaGa_4Se_7$ crystal. The light propagates along the *a* direction with E || *b* (red) and E || *c** (blue). The optical path length is 2.45 mm.

absorption bands peaking in the near-infrared with small oscillator strengths.[45]

The large 7 mT width of the trapped hole's EPR signal is a result of unresolved hyperfine interactions with ^{69}Ga and ^{71}Ga

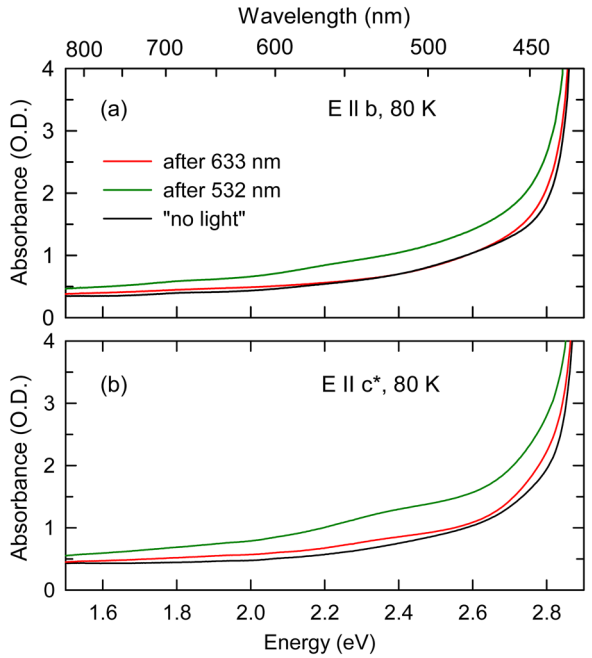

FIG. 10. Optical absorption spectra taken at 80 K from a $BaGa_4Se_7$ crystal. Light propagates along the *a* direction with (a) E || *b* and (b) E || *c**. Spectra were taken before exposure to laser light (black), after exposure to 532 nm laser light (green), and after exposure to 633 nm laser light (red).

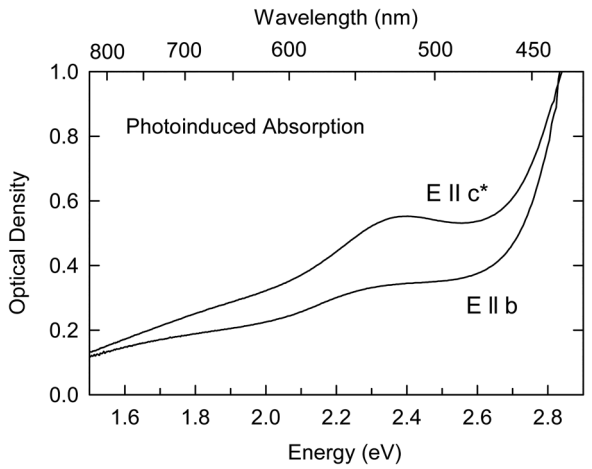

FIG. 11. Difference curves obtained from the 80 K spectra in Fig. 10. The spectrum taken before exposure to 532 nm light has been subtracted from the spectrum taken after exposure to 532 nm light. Light propagated along the *a* direction and was polarized either E || *b* and E || *c**. Absorption bands in the 520–530 and 710 nm regions, as well as near the band edge, are produced by the 532 nm laser light.

nuclei adjacent to the Se ion with the hole. Because of the lack of hyperfine information, we cannot say with certainty which vacancy, Ba^{2+} or Ga^{3+}, is responsible for stabilizing the hole on the selenium ion. However, a plausible argument can be made that we are seeing holes trapped by Ba^{2+} vacancies. The low thermal decay temperature (near 70 K) of the trapped hole is the critical information. The electrostatic binding energy, which is reflective of the activation energy for release of the hole, is expected to be smaller for the Ba^{2+} vacancy than for the Ga^{3+} vacancy. This expectation is based on the smaller effective negative charge (2−) of the doubly ionized Ba vacancy (V_{Ba}^{2-}) and the greater separation distance between the Se and Ba ions. For perspective, a hole trapped on an oxygen ion adjacent to a Ga vacancy in $LiGaO_2$ crystals is thermally stable at room temperature for more than one year.[46] A hole localized on one oxygen ion next to a Ga vacancy in β-Ga_2O_3 crystals is also stable at room temperature.[47]

IV. OPTICAL ABSORPTION RESULTS

Polarized optical absorption spectra were taken from the as-grown $BaGa_4Se_7$ crystal. The light propagated along the *a* direction and the optical path length was 2.45 mm. The shift of the band edge with temperature is shown in Fig. 9. At room temperature (296 K), the absorption edge occurs near 470 nm with a small shift to longer wavelength when the light is polarized E || *b* rather than E || *c**. Cooling the crystal to 80 K shifts the band edge to near 430 nm and reduces the energy separation between the absorption edges for E || *b* and E || *c**. A defect-related absorption feature near 450 nm in the 80 K data shows a polarization preference for E || *c**.

Exposing the $BaGa_4Se_7$ crystal to 532 nm laser light while at 80 K introduced broad optical absorption bands covering the visible region and extending slightly into the near-infrared.

Figure 10 shows the polarized absorption spectra obtained before the 532 nm illumination and immediately after removing the 532 nm light. Figures 10(a) and 10(b) are the spectra taken with $E \parallel b$ and with $E \parallel c^*$, respectively. These photoinduced absorption features thermally decayed within an hour when the crystal was left in the dark at 80 K. In contrast, applying 633 nm laser light at 80 K quickly destroyed (in a few seconds) nearly all the absorption that had been produced by the 532 nm light. The spectra taken after the exposure to the 633 nm light are also shown in Fig. 10.

Figure 11 shows absorption bands induced at 80 K by the 532 nm light. The two curves in this figure are difference spectra where the "before 532 nm light" spectrum has been subtracted from the "after 532 nm light" spectrum. Bands peaking near 520 nm ($E \parallel c^*$), 530 nm ($E \parallel b$), and 710 nm (both polarizations) are present. Additional photoinduced absorption extends beyond 440 nm on the short wavelength side and to near 1.2 μm on the long wavelength side. We suggest that the bands in the 520–530 nm region are intracenter transitions of the singly ionized selenium vacancies observed with EPR and the band near 710 nm is caused, in part, by the holes trapped at barium vacancies (i.e., the small polarons described in Sec. III C). The optical absorption bands and the EPR spectra are both produced by the 532 nm laser light, and they are both destroyed by the 633 nm laser light. Attributing an optical absorption band to a specific selenium vacancy EPR spectrum, however, must await more detailed studies of a larger set of $BaGa_4Se_7$ crystals grown under varying conditions and subjected to post-growth treatments.

V. SUMMARY

Electron paramagnetic resonance (EPR) has been used to identify and characterize singly ionized selenium vacancies (V_{Se}^{+}) in $BaGa_4Se_7$ crystals. The doubly ionized selenium vacancies (V_{Se}^{2+}) initially present in as-grown crystals are converted to their optically active paramagnetic charge state with 532 nm laser light. Five EPR spectra are observed, each representing a different vacancy site among the seven inequivalent sites in this monoclinic crystal and each showing large ^{69}Ga and ^{71}Ga hyperfine interactions. Holes localized on a selenium ion next to a cation vacancy, most likely a Ba^{2+} vacancy, are also seen with EPR. Optical absorption bands in the visible and near-infrared regions are produced at 80 K with 532 nm light. These bands, attributed to singly ionized selenium and barium vacancies, are expected to contribute to two-photon absorption and also direct one-photon absorption when an OPO is pumped near 1 μm. We suggest that post-growth annealing in a BaSe atmosphere may remove these vacancies and improve the performance of $BaGa_4Se_7$ crystals.

ACKNOWLEDGMENTS

T.D.G. was supported at the Air Force Institute of Technology by an NRC Research Associateship Award. Any opinions, findings, and conclusions or recommendations expressed in this paper are those of the authors and do not necessarily reflect the views of the United States Air Force.

AUTHOR DECLARATIONS

Conflict of Interest

The authors have no conflicts to disclose.

DATA AVAILABILITY

The data that support the findings of this study are available within the article.

REFERENCES

[1]V. Petrov, "Frequency down-conversion of solid-state laser sources to the mid-infrared spectral range using non-oxide nonlinear crystals," Prog. Quantum Electron. **42**, 1 (2015).
[2]X. Luo, Z. Li, Y. Guo, J. Yao, and Y. Wu, "Recent progress on new infrared nonlinear optical materials with application prospect," J. Solid State Chem. **270**, 674 (2019).
[3]A. Abudurusuli, J. Li, and S. Pan, "A review on the recently developed promising infrared nonlinear optical materials," Dalton Trans. **50**, 3155 (2021).
[4]V. Petrov, V. V. Badikov, D. V. Badikov, K. Kato, G. S. Shevyrdyaeva, K. Miyata, M. Mero, L. Wang, Z. Heiner, and V. L. Panyutin, "Barium nonlinear optical crystals for the mid-IR: Characterization and some applications," J. Opt. Soc. Am. B **38**, B46 (2021).
[5]S. Slussarenko and G. J. Pryde, "Photonic quantum information processing: A concise review," Appl. Phys. Rev. **6**, 041303 (2019).
[6]S. Krastanov, M. Heuck, J. H. Shapiro, P. Narang, D. R. Englund, and K. Jacobs, "Room-temperature photonic logical qubits via second-order nonlinearities," Nat. Commun. **12**, 191 (2021).
[7]J. Yao, D. Mei, L. Bai, Z. Lin, W. Yin, P. Fu, and Y. Wu, "$BaGa_4Se_7$: A new congruent-melting IR nonlinear optical material," Inorg. Chem. **49**, 9212 (2010).
[8]V. Badikov, D. Badikov, G. Shevyrdyaeva, A. Tyazhev, G. Marchev, V. Panyutin, V. Petrov, and A. Kwasniewski, "Phase-matching properties of $BaGa_4S_7$ and $BaGa_4Se_7$: Wide-bandgap nonlinear crystals for the mid-infrared," Phys. Status Solidi RRL **5**, 31 (2011).
[9]F. Yang, J. Yao, H. Xu, K. Feng, W. Yin, F. Li, J. Yang, S. Du, Q. Peng, J. Zhang, D. Cui, Y. Wu, C. Chen, and Z. Xu, "High efficiency and high peak power picosecond mid-infrared optical parametric amplifier based on $BaGa_4Se_7$ crystal," Opt. Lett. **38**, 3903 (2013).
[10]E. Boursier, P. Segonds, B. Ménaert, V. Badikov, V. Panyutin, D. Badikov, V. Petrov, and B. Boulanger, "Phase-matching directions and refined Sellmeier equations of the monoclinic acentric crystal $BaGa_4Se_7$," Opt. Lett. **41**, 2731 (2016).
[11]N. Y. Kostyukova, A. A. Boyko, V. Badikov, D. Badikov, G. Shevyrdyaeva, V. Panyutin, G. M. Marchev, D. B. Kolker, and V. Petrov, "Widely tunable in the mid-IR $BaGa_4Se_7$ optical parametric oscillator pumped at 1064 nm," Opt. Lett. **41**, 3667 (2016).
[12]K. Kato, K. Miyata, and V. Petrov, "Phase-matching properties of $BaGa_4Se_7$ for SHG and SFG in the 0.901–10.5910 μm range," Appl. Opt. **56**, 2978 (2017).
[13]D. B. Kolker, N. Y. Kostyukova, A. A. Boyko, V. V. Badikov, D. V. Badikov, A. G. Shadrintseva, N. N. Tretyakova, K. G. Zenov, A. A. Karapuzikov, and J.-J. Zondy, "Widely tunable (2.6–10.4 μm) $BaGa_4Se_7$ optical parametric oscillator pumped by a Q-switched Nd:$YLiF_4$ laser," J. Phys. Commun. **2**, 035039 (2018).
[14]G. Liu, Y. Chen, Z. Li, K. Yang, B. Yao, J. Yao, R. Wang, C. Yang, S. Mi, T. Dai, and X. Duan, "High-beam-quality 2.1 μm pumped mid-infrared type-II phase-matching $BaGa_4Se_7$ optical parametric oscillator with a $ZnGeP_2$ amplifier," Opt. Lett. **45**, 3805 (2020).
[15]D. Xu, J. Zhang, Y. He, Y. Wang, J. Yao, Y. Guo, C. Yan, L. Tang, J. Li, K. Zhong, Y. Wu, and J. Yao, "High-energy, tunable, long-wave mid-infrared optical parametric oscillator based on $BaGa_4Se_7$ crystal," Opt. Lett. **45**, 5287 (2020).

[16]F. Yang, J.-Y. Yao, Y.-W. Guo, L. Yuan, Y. Bo, Q.-J. Peng, D.-F. Cui, Y.-C. Wu, and Z.-Y. Xu, "High-energy continuously tunable 8–14 μm picosecond coherent radiation generation from BGSe-OPA pumped by 1064 nm laser," Opt. Laser Technol. **125**, 106040 (2020).
[17]K. Yang, G. Liu, C. Li, B. Yao, J. Yao, Y. Chen, S. Mi, X. Duan, and T. Dai, "Research on performance improvement technology of a $BaGa_4Se_7$ mid-infrared optical parametric oscillator," Opt. Lett. **45**, 6418 (2020).
[18]Y. Zhang, Y. Zuo, Z. Li, B. Wu, J. Yao, and Y. Shen, "High energy mid-infrared laser pulse output from a $BaGa_4Se_7$ crystal-based optical parametric oscillator," Opt. Lett. **45**, 4595 (2020).
[19]B. N. Carnio, E. Hopmann, K. T. Zawilski, P. G. Schunemann, and A. Y. Elezzabi, "Dependence on excitation polarization and crystal orientation for terahertz radiation generation in a $BaGa_4Se_7$ crystal," Opt. Express **28**, 15016 (2020).
[20]B. N. Carnio, K. T. Zawilski, P. G. Schunemann, and A. Y. Elezzabi, "Generation of narrowband terahertz radiation via phonon mode enhanced nonlinearities in a $BaGa_4Se_7$ crystal," Opt. Lett. **45**, 4722 (2020).
[21]Y. Yin, B. Wang, Yiwen E, J. Yao, L. Wang, X. Bai, and W. Liu, "Raman spectra and phonon structures of $BaGa_4Se_7$ crystal," Commun. Phys. **3**, 34 (2020).
[22]Yiwen E, J. Yao, and L. Wang, "Propagation of terahertz waves in a monoclinic crystal $BaGa_4Se_7$," Sci. Rep. **8**, 16229 (2018).
[23]J. Yao, W. Yin, K. Feng, X. Li, D. Mei, Q. Lu, Y. Ni, Z. Zhang, Z. Hu, and Y. Wu, "Growth and characterization of $BaGa_4Se_7$ crystal," J. Cryst. Growth **346**, 1 (2012).
[24]Y. Guo, Z. Li, Z. Lei, X. Luo, J. Yao, C. Yang, and Y. Wu, "Synthesis, growth of crack-free large-size $BaGa_4Se_7$ crystal, and annealing studies," Cryst. Growth Des. **19**, 1282 (2019).
[25]N. Y. Kostyukova, A. A. Boyko, E. Y. Erushin, A. I. Kostyukov, V. V. Badikov, D. V. Badikov, and D. B. Kolker, "Laser-induced damage threshold of $BaGa_4Se_7$ and $BaGa_2GeSe_6$ nonlinear crystals at 1.053 μm," J. Opt. Soc. Am. B **36**, 2260 (2019).
[26]N. Y. Kostyukova, A. A. Boyko, I. D. Eranov, O. L. Antipov, D. B. Kolker, A. I. Kostyukov, E. Y. Erushin, I. B. Miroshnichenko, D. V. Badikov, and V. V. Badikov, "Laser-induced damage threshold of the nonlinear crystals $BaGa_4Se_7$ and $BaGa_2GeSe_6$ at 2091 nm in the nanosecond regime," J. Opt. Soc. Am. B **37**, 2655 (2020).
[27]J.-M. Spaeth and H. Overhof, *Point Defects in Semiconductors and Insulators: Determination of Atomic and Electronic Structure From Paramagnetic Hyperfine Interactions* (Springer-Verlag, Berlin, 2003).
[28]J. A. Weil and J. R. Bolton, *Electron Paramagnetic Resonance: Elementary Theory and Practical Applications*, 2nd ed. (John Wiley and Sons, Hoboken, NJ, 2007).
[29]*EPR Spectroscopy: Fundamentals and Methods*, edited by D. Goldfarb and S. Stoll (John Wiley and Sons, Chichester, 2018).
[30]A. P. Yelisseyev, S. I. Lobanov, P. G. Krinitsin, and L. I. Isaenko, "The optical properties of the nonlinear crystal $BaGa_4Se_7$," Opt. Mater. **99**, 109564 (2020).
[31]P. G. Schunemann and K. T. Zawilski, "Horizontal gradient freeze growth of wide band gap mid-infrared NLO crystals $BaGa_4S_7$ and $BaGa_4Se_7$," Proc. SPIE **10516**, 105160T (2018).
[32]R. D. Shannon, "Revised effective ionic radii and systematic studies of interatomic distances in halides and chalcogenides," Acta Cryst. A **32**, 751 (1976).
[33]N. J. Stone, "Table of nuclear magnetic dipole and electric quadrupole moments," At. Data Nucl. Data Tables **90**, 75 (2005).
[34]S. Stoll and A. Schweiger, "EasySpin, a comprehensive software package for spectral simulation and analysis in EPR," J. Magn. Reson. **178**, 42 (2006).
[35]See https://www.easyspin.org for the EasySpin program.
[36]G. Breit and I. I. Rabi, "Measurement of nuclear spin," Phys. Rev. **38**, 2082 (1931).
[37]I. I. Rabi, "On the process of space quantization," Phys. Rev. **49**, 324 (1936).
[38]J. A. Weil, "The analysis of large hyperfine splitting in paramagnetic resonance spectroscopy," J. Magn. Reson. **4**, 394 (1971).
[39]A. Räuber and J. Schneider, "Electron spin resonance of a photosensitive $^2S_{1/2}$-state gallium center in ZnS," Phys. Rev. Lett. **16**, 1075 (1966).
[40]G. E. Holmberg, K. H. Lee, and J. H. Crawford, Jr., "EPR and optical studies of γ-irradiated MgO:Ga," Phys. Rev. B **19**, 2436 (1979).
[41]S. V. Nistor, D. Schoemaker, and I. Ursu, "Spectroscopy of the ns^1-centers in ionic crystals," Phys. Status Solidi B **185**, 9 (1994).
[42]D. V. Azamat, A. Dejneka, J. Lancok, V. A. Trepakov, L. Jastrabik, and A. G. Badalyan, "Electron paramagnetic resonance studies of manganese centers in $SrTiO_3$: Non-Kramers Mn^{3+} ions and spin-spin coupled Mn^{4+} dimers," J. Appl. Phys. **111**, 104119 (2012).
[43]R. A. Serway, W. Berlinger, K. A. Müller, and R. W. Collins, "Electron paramagnetic resonance of three manganese centers in reduced $SrTiO_3$," Phys. Rev. B **16**, 4761 (1977).
[44]H. J. Gerritsen and E. S. Sabisky, "Paramagnetic resonance of trivalent manganese in rutile (TiO_2)," Phys. Rev. **132**, 1507 (1963).
[45]O. F. Schirmer, "O^- bound small polarons in oxide materials," J. Phys.: Condens. Matter **18**, R667 (2006).
[46]C. A. Lenyk, M. S. Holston, B. E. Kananen, L. E. Halliburton, and N. C. Giles, "Lithium and gallium vacancies in $LiGaO_2$ crystals," J. Appl. Phys. **124**, 135702 (2018).
[47]B. E. Kananen, L. E. Halliburton, K. T. Stevens, G. K. Foundos, and N. C. Giles, "Gallium vacancies in β-Ga_2O_3 crystals," Appl. Phys. Lett. **110**, 202104 (2017).
[48]M. S. Holston, J. W. McClory, N. C. Giles, and L. E. Halliburton, "Radiation-induced defects in $LiAlO_2$ crystals: Holes trapped by lithium vacancies and their role in thermoluminescence," J. Lumin. **160**, 43 (2015).
[49]M. W. Swinney, J. W. McClory, J. C. Petrosky, S. Yang, A. T. Brant, V. T. Adamiv, Ya. V. Burak, P. A. Dowben, and L. E. Halliburton, "Identification of electron and hole traps in lithium tetraborate ($Li_2B_4O_7$) crystals: Oxygen vacancies and lithium vacancies," J. Appl. Phys. **107**, 113715 (2010).